Surface Modification Effects of Core–Shell Rubber Particles on the Toughening of Poly(butylene terephthalate)

Hoichang Yang,* Kilwon Cho

Department of Chemical Engineering, Pohang University of Science and Technology, Pohang 790-784, South Korea

Received 22 September 2008; accepted 13 September 2009
DOI 10.1002/app.31434
Published online 7 January 2010 in Wiley InterScience (www.interscience.wiley.com).

ABSTRACT: We toughened poly(butylene terephthalate) (PBT) by loading core–shell rubber (CSR) type impact modifiers, consisting of a rubbery poly(*n*-butyl acrylate) core and a rigid poly(methyl methacrylate) shell. To optimize the dispersion of CSR particles into the PBT matrix during melt compounding, the shell surface was modified with different grafting ratios of glycidyl methacrylate (GMA) reactive with PBT chain ends. In PBT blends with a 20 wt % CSR loading, the dispersed rubbery phases showed discernible shapes depending on the grafted GMA content, from predetermined spheres with 0.25 ± 0.05 μm diameters to their aggregates in the 2–3 μm diameter range. As a result, the interparticle spacing (τ) could be controlled from 0.25 to 4.0 μm in the PBT blends containing the fixed rubber loading. The Izod impact strengths of these samples increased significantly below $\tau = 0.4$ μm. Additional thermal and morphological analyses strongly supported the hypothesis that the marked increase in toughness of the blends was related to less ordered lamellar formation of the PBT matrix under the confined geometry. © 2010 Wiley Periodicals, Inc. J Appl Polym Sci 116: 1948–1957, 2010

Key words: core–shell polymers; morphology; polyesters; structure–property relations; toughness

INTRODUCTION

Semicrystalline poly(butylene terephthalate) (PBT) is one of the most prevalent engineering plastics used in the automotive and construction industries. Because its properties include notch sensitivity, brittleness, and low wear resistance, PBT is often blended with rubbery fillers as an efficient way to improve its physical properties.[1–9] The main factors affecting the properties of rubber-modified semicrystalline polymer blends are as follows: (1) rubbery content and size, (2) rubber properties, (3) crystalline structure and morphologies of the blends, (4) dispersed interparticle spacing (τ), and (5) the rubber–polymer interface.

Among rubbery impact modifiers, core–shell rubber (CSR) type fillers are commonly used for polymer toughening because of their predetermined size, as the domain sizes of other rubbers are hard to control because they are process-dependent. However, because of their incompatibility with polymer matrices, CSR fillers tend to aggregate with each other, especially in low-viscosity matrices. This agglomeration can be minimized by the use of a chemical reaction that directly links the matrix chains around the fillers during blending[9–11] or by the loading of a tertiary polymer that is physically compatible with both components.[12–14]

The brittle–ductile transition (BDT) of rubber-toughened semicrystalline polymers is known to be strongly correlated with τ, instead of with rubber content and size.[15] Wu[15] explained the BDT behavior in rubber-toughened polyamide 66 with a stress-field theory; under an applied load, it is related to the overlap of the stress field around the neighbor fillers, and the subsequent stress relaxation is induced by rubber cavities. The parameter τ has been considered one of the most influential factors in toughening and contributes to significant increases in the toughness of many semicrystalline polymers.[9,16–19] For high-density polyethylene (HDPE) blends containing either $CaCO_3$ or rubber fillers, Bartczak et al.[17,18] found that the toughness of these HDPE blends was dramatically improved below a critical value of interparticle spacing (τ_c) of 0.6 μm, regardless of which filler was used. In addition, with the use of HDPE films with various thicknesses on $CaCO_3$ and rubber substrates as simple model systems for $CaCO_3$/HDPE and rubber/HDPE blends,[20] it was found that, at a film thickness (*t*) of

**Present address:* Department of Advanced Fiber Engineering, Inha University, Yonghyun-Dong 253, Incheon 402-751, Korea.

Correspondence to: K. Cho (kwcho@postech.ac.kr.).

Contract grant sponsors: Ministry of Science and Technology of Korea (National Research Laboratory Program), Ministry of Education of Korea (BK21 Program).

less than $\tau_c/2$, crystalline lamellae in sheaflike HDPE spherulites were preferentially oriented with respect to both the $CaCO_3$ and the rubber substrates, whereas at $t > \tau_c/2$, they were randomly oriented with respect to the substrates. In contrast, Kanai et al.[19] reported that the τ_c values depended on the matrix crystallinity (ϕ_c) and the filler modulus in rubber-modified polymer blends, suggesting that τ_c is not a characteristic parameter of these materials. The loading of heterogeneous fillers significantly affects the crystallization behavior of semicrystalline polymer matrices.[21] Recently, we reported that, in nano-Al_2O_3/poly(ethylene terephthalate) nanocomposites, poly(ethylene terephthalate) crystallites were converted from three-dimensional (3-D) spherulites to prematured two-dimensional lamellae, through a decrease in τ.[21]

In this study, poly(*n*-butyl acrylate) (PBA)–poly (methyl methacrylate) (PMMA) CSR fillers with a predetermined size of about 0.40 μm were synthesized as impact modifiers for semicrystalline PBT. In PBT blends melt-compounded with 20 wt % CSR filler, τ could be controlled from 0.25 to 4.0 μm by different agglomerations of the CSR fillers resulting from different grafting ratios of glycidyl methacrylate (GMA) in the shell. For the controlled PBT blends, we investigated the overall morphologies, crystallization behaviors, crystalline structures, and impact strengths by using differential scanning calorimetry (DSC), transmission electron microscopy (TEM), and Izod impact testing.

EXPERIMENTAL

Sample preparation

PBT (number-average molecular weight = 36,000 g/mol) was obtained from Samyang Industry (Daejeon, Korea). Methyl methacrylate and *n*-butyl acrylate were obtained from Aldrich (USA) and were used after the removal of inhibitors by several washings with a 10% aqueous NaOH solution. The initiators potassium persulfate and 2,2-azobisisobutyronitrile were obtained from Aldrich and were used without further purification. 1,4-Butanediol diacrylate (Merck, USA) and GMA (Merck) were used as a crosslinker for the rubbery core and a chemical compatibilizer between the fillers and PBT, respectively. CSR fillers containing a rubbery PBA core and a glassy PMMA shell were synthesized by a stepwise emulsion polymerization, where a shell component was subsequently polymerized on the outer surface of a predetermined core particle.[22] To maintain the chemical activity of the epoxide moieties in the grafted glycidyl methacrylates (*g*GMAs) around the outer shell surface, the final polymerization step was performed at about pH 7. The grafting ratios of GMA were controlled from 0 to 4 wt % of the PMMA shell. In the resulting CSR fillers, about 70% of *g*GMAs were chemically active by the titration method:[9] the epoxy group in the CSR was cleaved with an excess of HCl, and then the remaining HCl was back-titrated with KOH (0.1*N*). The resulting values corresponded to 0.2, 0.4, 0.7, and 0.85 wt % in the fillers, respectively. Figure 1 displays the scanning electron microscopy (Hitachi S-4200, Japan) images of the CSR fillers. All CSR particles showed uniform size distributions of about 0.40 μm; this was less dependent on their *g*GMA content, with the size of the rubbery cores indicated as 0.25–0.27 μm (Table I) on the basis of a core-to-shell volume ratio of 7 : 3.

PBT and the CSR fillers were sufficiently dried in a vacuum oven at 140 and 40°C, respectively. PBT was then melt-compounded with 20 wt % CSR filler with an internal mixer (Brabender, USA) at 240°C for 5 min. The rubber-modified PBT blends were remelted and compression-molded into a 5 mm thick plate at a cooling rate of 10°C/min. Finally, the molded samples were machined into impact bars according to ASTM D 261 requirements.

Characterization

To systematically investigate the crystallization behaviors in the molten PBT blends and the melting behaviors of the corresponding PBT crystals, DSC (PerkinElmer 7, USA) was performed with a cooling rate of 10°C/min and a subsequent heating rate of 10°C/min. The Izod impact strength of the specimens was measured at room temperature. Bulk and fractured blend morphologies were observed under TEM (JEOL 1200EX, Japan), with an accelerating voltage of 120 kV. TEM samples were prepared with a cryogenic ultramicrotoming system (RMC, MT-7000, USA) with a diamond knife at − 70°C. In particular, to examine the fracture behavior in the PBT blend, Izod impact tested samples were embedded into an epoxy kit (Polybed 812, Polysciences, USA), which was completely cured at 60°C for 24 h. Finally, three different zones around the crack were collected along the direction normal to the fractured surface. All sectioned films were picked up on 300-mesh copper grids. To enhance the TEM image contrast for the PBT blends, the PBT matrix and the CSR fillers were selectively stained with 0.5 wt % aqueous ruthenium tetraoxide (RuO_4)[23] and 1.0 wt % osmium tetraoxide (OsO_4) solutions,[24] respectively.

RESULTS AND DISCUSSION

The physical properties of filler-loaded polymer blends are strongly affected by the filler dispersion and filler–matrix interface properties. The CSR surface used in this study was not sufficiently

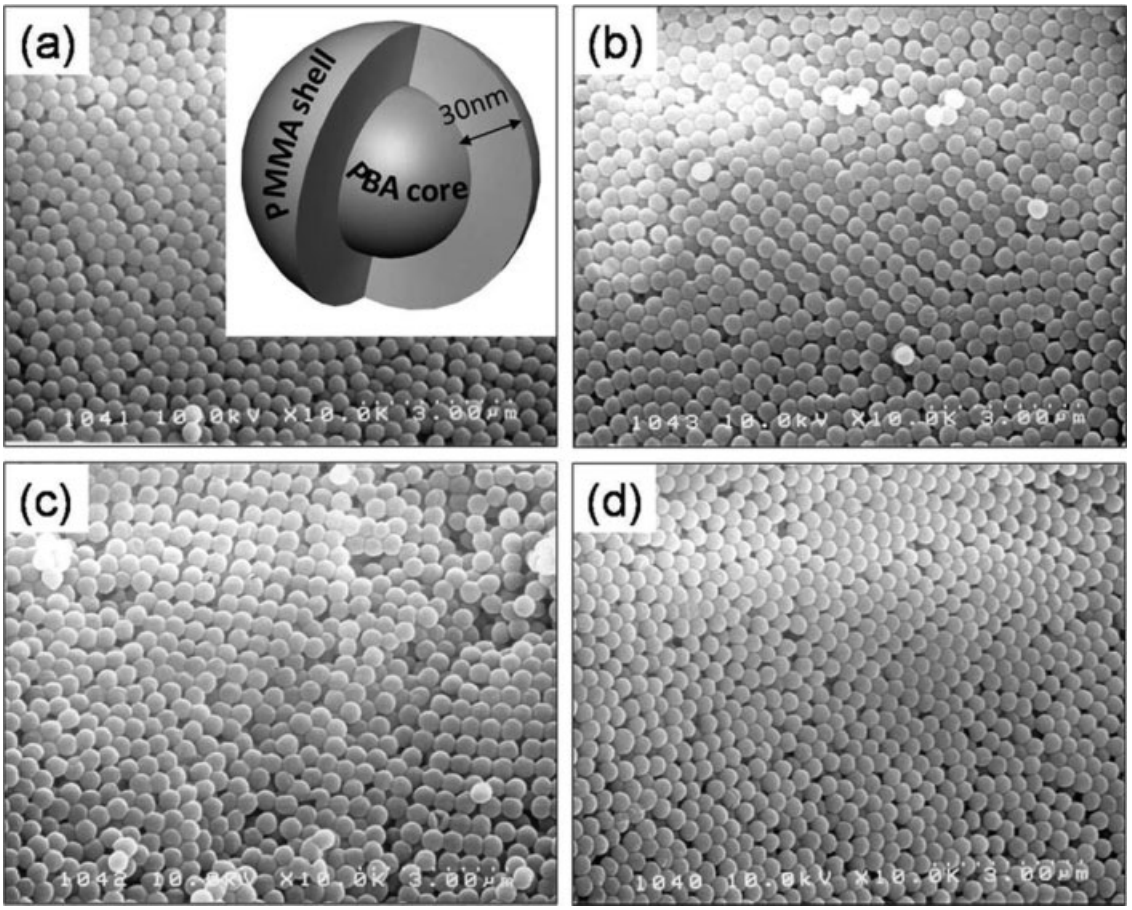

Figure 1 Scanning electron micrographs of CSR fillers with various *g*GMA contents: (a) 0, (b) 0.2, (c) 0.4, and (d) 0.7 wt %, respectively.

compatible with the PBT matrix, with the anticipated agglomeration of the CSR fillers in the low-viscosity PBT melt.[9] By changing the grafting ratios of GMA around the PMMA shell, however, we could control the filler dispersion and aggregate size in the PBT blends because hydroxyl (—OH) and/or carboxyl (—COOH) moieties on the PBT chain ends could react with the epoxide moiety in *g*GMA during melt compounding. The moiety —OH tends to attack the more substituted carbons of the epoxide group, whereas —COOH attacks the less substituted carbons. These reactions could induce tethering of the PBT chains on the CSR surface.[1,3,5,8]

Blend morphology

CSR-loaded blends (20 wt %) were melted at 240°C and compression-molded with a cooling rate of 10°C/min. Figure 2 represents typical TEM morphologies of the pure PBT and PBT blends containing discernible rubbery phases, dependent on the *g*GMA content in the fillers. As shown in Figure 2, amorphous PBT regions and acryl-based fillers were stained selectively with RuO_4 and OsO_4 staining agents, respectively, although the mechanism of the selective staining was not clear.[23,24] In the pure melt-crystallized PBT, PBT lamellae tended to grow radially from a nucleation site until they impinged against growing lamellae at nearby nucleation sites; this resulted in 3-D spherulites 15–20 μm in diameter [Fig. 2(a)]. In contrast, the PBT blend morphologies were significantly changed by the presence of *g*GMA in the fillers. During melt blending, the low-viscosity PBT matrix first agglomerated the CSR fillers without *g*GMA. Aggregates with average particle diameters (D_{ave}) of 2.4 ± 0.9 μm were indicated as rubbery phases containing migrated PBT phases by the TEM

TABLE I
Characterization of CSR Fillers Containing Different *g*GMA Contents

CSR filler	gGMA content (wt %)	Diameter (nm)	
		Overall	Core
1		370 ± 24	248 ± 16
2	0.20	404 ± 16	270 ± 11
3	0.40	410 ± 20	274 ± 14
4	0.70	382 ± 20	256 ± 13
5	0.85	389 ± 18	260 ± 12

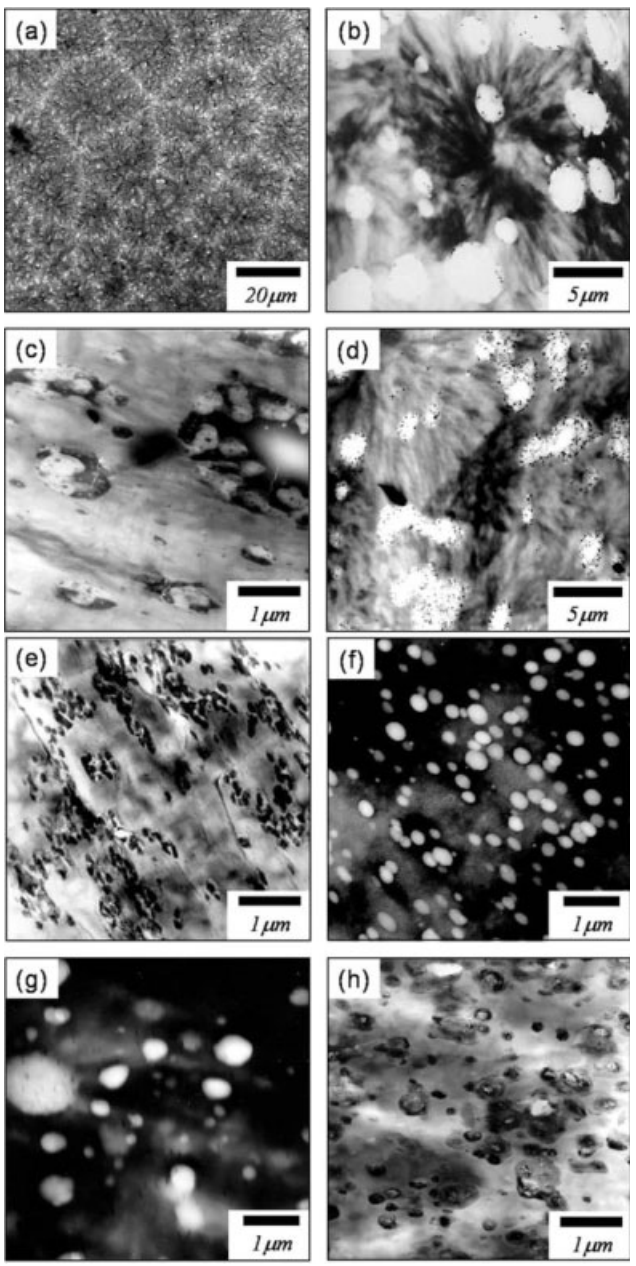

Figure 2 TEM micrographs of the pure PBT and PBT blends containing 20 wt % CSR fillers with various *g*GMA contents: (a) pure PBT, (b,c) 0 wt % *g*GMA, (d,e) 0.2 wt % *g*GMA, (f) 0.4 wt % *g*GMA, and (g,h) 0.7 wt % *g*GMA. (Note that the TEM contrast in parts (a), (b), (d), (f), and (g) was increased by the staining of the amorphous PBT components with RuO_4, whereas that in parts (c), (e), and (h) was increased by the staining of the fillers with OsO_4.)

micrographs [Fig. 2(b,c)]; the dark and white contrast areas in the aggregates corresponded to merged CSR fillers and PBT phases, respectively. *g*GMA fillers (0.2 wt %) were less agglomerated in the blend and showed showing aggregates [$D_{ave} = 1.6 \pm 0.8$ μm; Fig. 2(d)]. Unlike the 0 wt % *g*GMA filler, the CSR fillers retained their predetermined sphere in the aggregates, as shown in Figure 2(e). Finally, although 0.4 wt % *g*GMA fillers were individually dispersed in the blend [Fig. 2(f)], further GMA grafting again aggregated the fillers in the blends. The results strongly support the notion that the presence of *g*GMA around the CSR surfaces improved the stability and dispersion of the fillers during melt blending with PBT, but an optimum grafting ratio was required to individually disperse the CSR particles. Hale and coworkers[10,11,25] reported similar results for acrylonitrile butadiene styrene (ABS)/PBT blends with the assistance of methyl methacrylate–GMA–ethyl acrylate terpolymer.

Figure 3 illustrates potential reactions of *g*GMA in the fillers with free PBT chain ends during melt blending. We expected to find that the presence of *g*GMA around the CSR surfaces would yield tethered PBT chains on the filler surfaces[1,3,5,8] and result in the stabilization of the fillers in the low-viscosity PBT melt. In the presence of excessive *g*GMA around the fillers, however, the active epoxide moieties around some CSR fillers reacted with both free PBT chain ends and the ends of other tethered PBT chains because the loaded fillers were very close to each other in the initial mixing state and yielded aggregated fillers interconnected by bridged PBT chains [Fig. 3(b)]. As a result, we suggest the hypothesis that the competition between the two different chemical reactions yielded various mesoscale morphologies in the 20 wt % CSR filler-loaded PBT blends, depending on the level of GMA loading.

On the basis of the TEM analysis of the rubber-toughened PBT blends, Figure 4(a) shows D_{ave} of the rubbery phases as a function of *g*GMA content in the filler; D_{ave} values in the PBT blends changed dramatically from about 0.25 to 2.4 ± 0.9 μm. These variations induced significant changes in τ in the blends with the same CSR loadings of 20 wt % [Fig. 4(b)]. The D_{ave}–τ relationship calculated from all of the PBT blends closely matched the theoretical τ values in ideal blends with the same volume fraction of spherical fillers [solid line in Fig. 4(b)].[26]

In filler-loaded semicrystalline polymer blends, a decrease in τ significantly increases the geometrical confinement and thereby affects the chain mobility of the polymers and, thus, the crystal growth.[20] As shown in Figure 2(b,d), in the 0 and 0.2 wt % *g*GMA filler-loaded samples with $\tau > 1$ μm, the PBT crystallites grew into 3-D spherulites with trapped rubbery phases, although the spherulitic sizes decreased considerably with decreasing τ. In contrast, the PBT blends with $\tau < 1$ μm contained no spherulitic crystallites [Fig. 2(f–h)]. Semicrystalline polymer thin films with various thicknesses are considered to be ideal model systems for investigating polymer crystallization under physical confinement. At critical film thicknesses from 100 nm to 1 μm, the crystal growth mode of polymers starts to change from

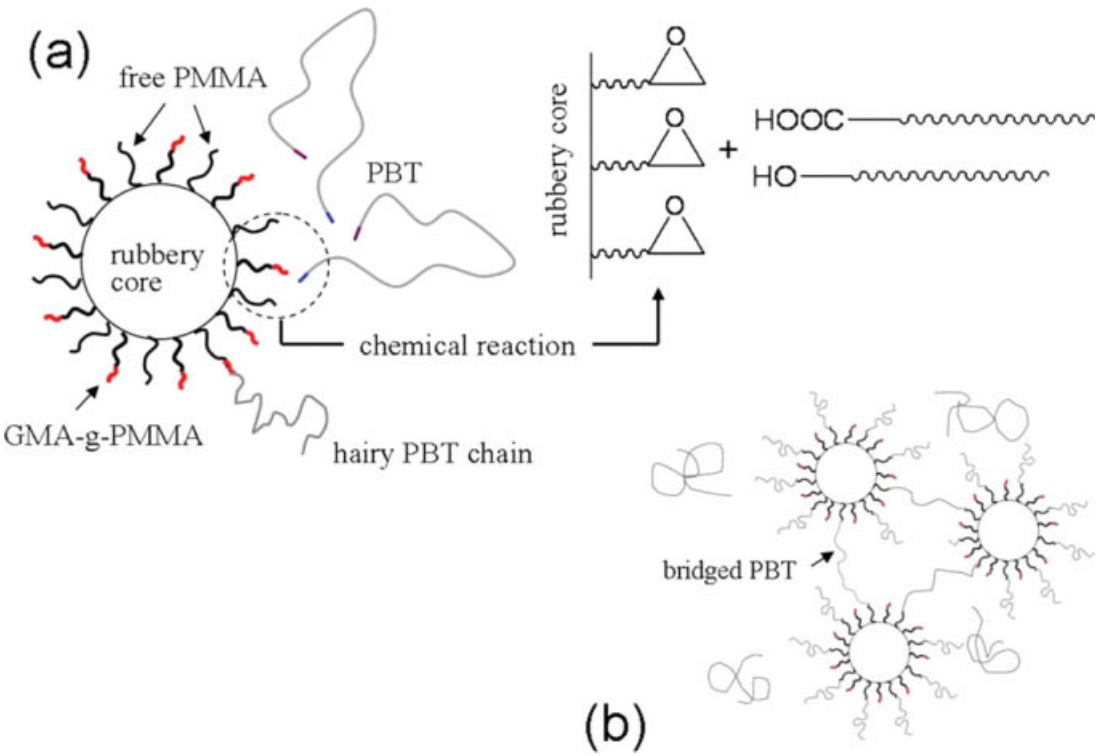

Figure 3 Schematic diagrams of the potential reactions between *g*GMA and the PBT chains around the fillers. [Color figure can be viewed in the online issue, which is available at www.interscience.wiley.com.]

isotropic 3-D to preferentially oriented two-dimensional with respect to the substrate; this results in edge-on lamellar sheaves[27–30] or flat-on crystals[27,28] in films. For both filler-loaded HDPE blends and HDPE films with controlled confinements, Bartczak and coworkers[17,18,20] reported on the τ-dependent growth transition of HDPE in the blends observed in the confined films as a function of a film thickness of τ/2.

For the rubber-toughened PBT blends used in this study, we expected that tethered PBT chains, by potential reaction with *g*GMAs on the filler surface, would affect the nucleation behavior of PBT. Comparing the lamellar morphologies in the pure PBT and PBT blends (Fig. 5), we found, in fact no clear evidence for the anisotropic lamellar growth of PBT around the dispersed fillers. The bulk morphology of pure PBT showed randomly growing lamellae with thicknesses of 10–15 nm [Fig. 5(a)]. For the PBT blends, the 0.4 wt % *g*GMA filler sample seemed to contain anisotropic lamellae grown normal to the particle surface [see the circular area in Fig. 5(b)], but there was no clear evidence of a preferred lamellar orientation. Interestingly, most PBT lamellae in the 0.7 wt % *g*GMA sample ($\tau \approx 300$ nm) were more twisted and curled, especially around the particles.

Crystallization behaviors and lamellar structure of PBT

In filler-loaded semicrystalline polymer blends, chemistry changes in the loaded filler affect the crystal growth and structure of the matrix polymer.[31–34] One reason for these phenomena is related to the presence of different energy filler surfaces of the polymer; for example, a high-energy filler surface helps the polymer melt easily and solidify under only small supercooling conditions ($\Delta T = T_m - T_c$, where T_m is the melting peak temperature and T_c is the crystallization peak temperature). However, the essential mechanism of this process is still unclear. Given the potential reactions illustrated in Figure 3, the participation of the PBT chains tethered around the fillers in either nucleation or PBT crystalline/amorphous formation needs to be considered. DSC is a convenient tool for investigating the crystallization behaviors and average lamellar sizes (or perfection) of semicrystalline polymers. Like most semicrystalline polymers containing aromatic components, PBT exhibits multiple melting endotherms, depending on the annealing or crystallization conditions.[26,35–38]

Figure 6 shows the nonisothermal DSC curves of the pure PBT and the PBT blends measured from the melt at a cooling rate of 10°C/min and rescanned at a heating rate of 10°C/min. Table II lists the thermal characteristics of the samples. In terms of the crystallization kinetics, T_c of pure PBT was found to be 183°C; this was much lower than those of the PBT blends, which ranged from 188 to 191.5°C. For the PBT blends, the T_c values tended to increase monotonically with increasing *g*GMA

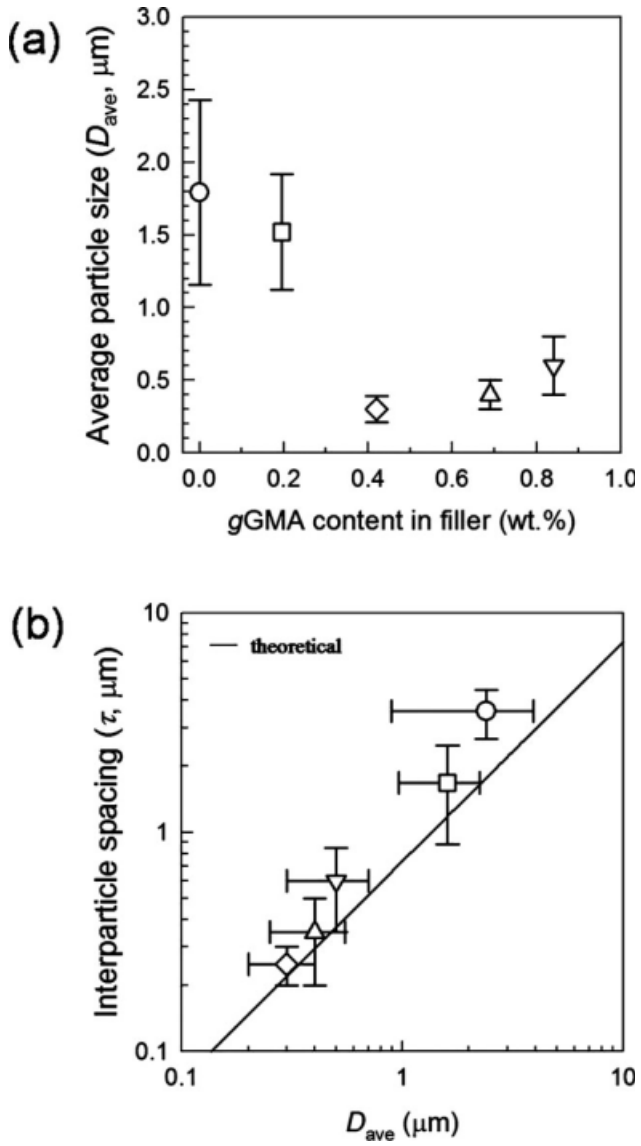

Figure 4 (a) Variation of D_{ave} of the PBT blends containing 20 wt % CSR fillers with the *g*GMA content. (b) τ versus D_{ave} in the PBT blends.

content in the CSR fillers. The results support the hypothesis that the PBT chains tethered around the fillers by the potential reaction between the PBT chain and *g*GMA provided extra nucleation sites, which required a lower ΔT compared to pure PBT. The DSC cooling curves were used to calculate sample ϕ_c, instead of the DSC heating curves, which often contain melting endotherms from recrystallized polymers. The ϕ_c values of the blends decreased monotonically from 0.29 to 0.23 as the *g*GMA content in the fillers increased and were lower compared to the 0.31 value of pure PBT. This result suggests that the geometrical confinement by the CSR loading interfered with the crystal growth and development of PBT.

DSC heating curves were obtained for all of the samples crystallized by the preceding cooling

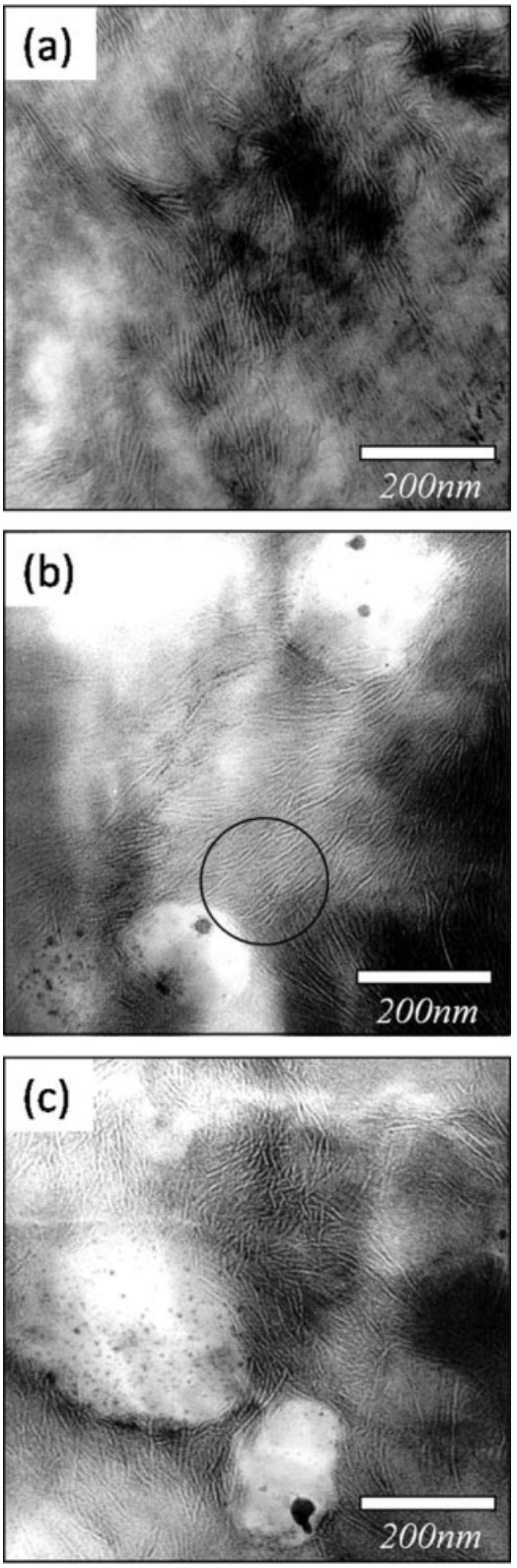

Figure 5 High-magnification TEM micrographs of pure PBT and the PBT blends: (a) pure PBT, (b) 0.4 wt % *g*GMA, and (c) 0.7 wt % *g*GMA filler-loaded PBT blend. (All scale bars are 200 nm.)

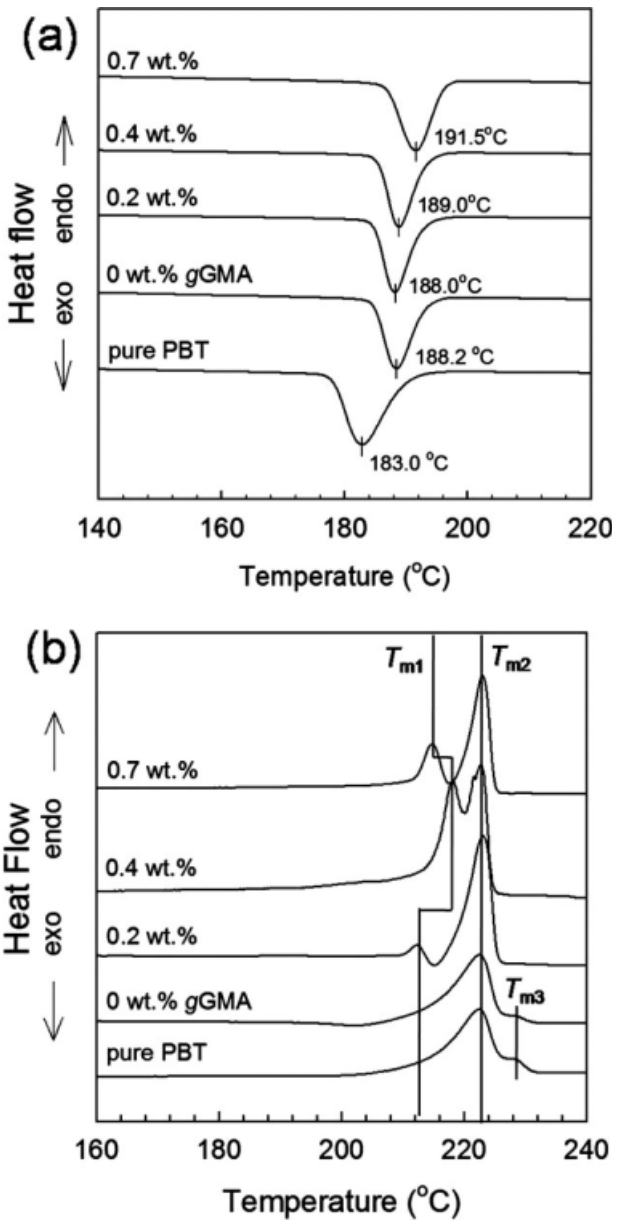

Figure 6 (a) DSC cooling and (b) subsequent heating curves of the samples measured with a rate of 10°C/min. (Before the nonisothermal melt crystallization, all samples were held at 250°C for 10 min.)

method. As shown in Figure 6(b), there existed three different types of melting endothermic peaks of the PBT crystals (T_{m1}, T_{m2}, and T_{m3}). In all of the samples, the melting endotherms of the PBT crystals near T_{m2} showed different breadths, depending on the loadings of the CSR fillers. However, their peak positions were indicated at the same T of about 223°C. For pure and 0 wt % *g*GMA filler-loaded PBT samples, small endothermic peaks were indicated at $T_{m3} \approx 228$°C. These were mainly related to the melting of crystals that regenerated during the DSC heating history.[26,35,36] Interestingly, for the PBT blends incorporating different *g*GMA contents, some portion of the PBT crystals started to melt, and their endothermic peaks indicated different T's ($<T_{m2}$) marked as T_{m1}, although the major melting endotherms were indicated near T_{m2}. Yeh and Runt[38] reported that a relatively lower melting endotherm in comparison to the major melting endotherm is associated with thinner lamellae formed near T_c.

In this study, both the peak position and portion of the low-melting endotherm tended to increase with the degree of dispersion of the CSR fillers. In particular, the 0.4 wt % *g*GMA filler-loaded blend showing well-dispersed CSR fillers ($\tau = 0.2$ μm) contained a large portion of the low-melting endotherm. The variations in the low-melting endotherm at T_{m1} were attributed to drastic changes in the confined blend geometry and the PBT/filler interface induced by different *g*GMA loadings: the modified CSR filler surfaces acted as heterogeneous nucleation sites, but the decrease in τ prevented PBT from growing into thicker and perfect crystals.

Fracture toughness and behavior

For many toughened semicrystalline polymer blends, a drastic increase in toughness, that is, a BDT, has been found to occur below τ_c, regardless of the physical properties, volume fraction, and size of the loaded fillers.[1,3–20,25,33,34,39] In this study, the impact strengths of the 20 wt % CSR filler-loaded PBT blends showing variations in τ were measured at room temperature. Figure 7 represents the measured impact strengths as functions of the *g*GMA content in the fillers and τ. As shown in Figure 7(a), the 0.4 wt % *g*GMA filler-loaded sample showed the highest impact strength ($\sim$ 210 J/m) by a factor of 12 greater than that of pure PBT ($\sim$ 17 J/m). By plotting the variation of the impact strength with τ [Fig. 7(b)], we found that the toughness of the rubber-modified PBT blends significantly improved with decreasing τ, especially for $\tau < 0.4$ μm. Arostegui and coworkers[4,5,16] reported a similar trend for PBT blends containing phenoxy- and maleic-grafted poly(ethylene–octene) rubbers. For PBT blends toughened with different types of fillers, however,

TABLE II
Thermal Properties and ϕ_c Values of the Pure PBT and PBT Blends

Sample	T_c (°C)	T_m (°C)			ϕ_c
		T_{m1}	T_{m2}	T_{m3}	
Pure PBT	183.0	—	223.1	228.0	0.31
0 wt % *g*GMA	188.2	—	222.8	228.2	0.29
0.2 wt % *g*GMA	188.0	214.4	223.4	—	0.28
0.4 wt % *g*GMA	189.0	218.1	222.9	—	0.25
0.7 wt % *g*GMA	191.5	216.3	222.9	—	0.23

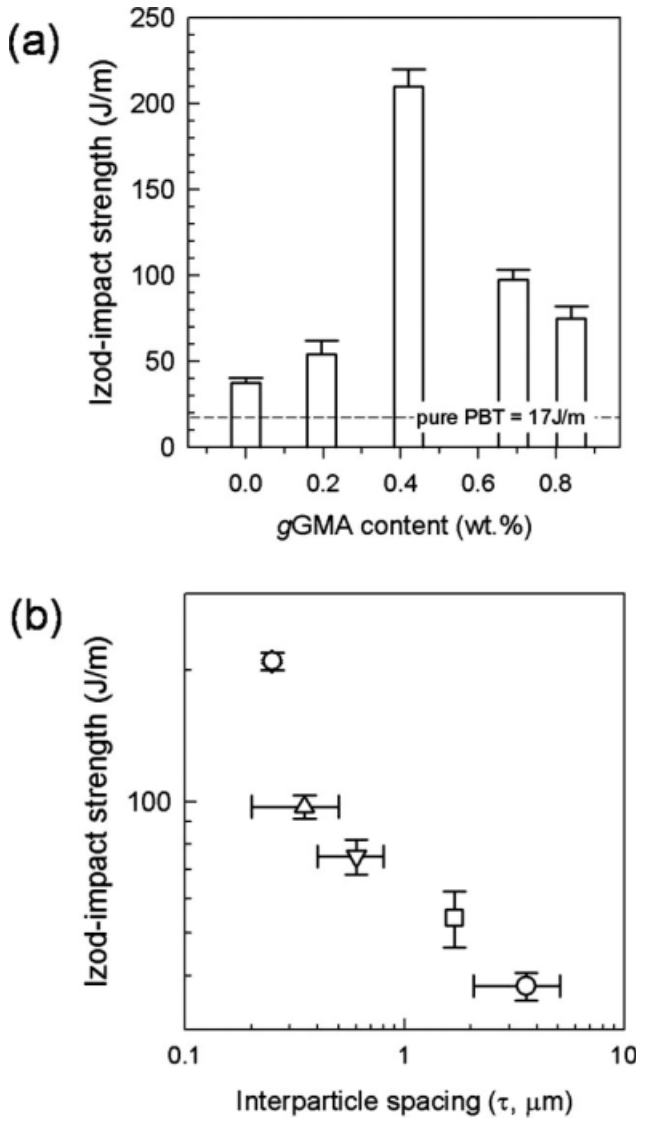

Figure 7 Izod impact strengths of the 20 wt % CSR-loaded PBT blends as a function of (a) *g*GMA content in the fillers and (b) τ.

Kanai et al.[19] reported that the BDT of the PBT blends was affected by the modulus of the fillers, for example, $\tau_c = 0.4$ μm for ethylene olefin rubber and $\tau_c = 0.16$ μm for styrene-ethylene/butadiene-styrene (SEBS) rubber. In addition, the BDT of semicrystalline polymer/filler blends was found to strongly depend on the matrix ϕ_c.

In applying stress at initial crack, the pure PBT samples containing typical 3-D spherulitic crystals showed low crack resistance; the sharp crack initially created propagated easily along the spherulitic boundaries. In the rubbery filler-loaded PBT blends, however, the crack seemed to be blunt, and its propagation rate became slower because of the large matrix deformation, which was indicated as a whitened area near the crack. To investigate the fracture behavior of rubber-toughened PBT blends during Izod impact testing, TEM analysis was performed for the 0.4 wt % *g*GMA filler-loaded samples reporting the highest impact strength.

Figure 8 shows the TEM micrographs of a PBT blend showing drastic changes of matrix deformation along the normal direction of the crack propagation around the notch tip. Regions I, II, and III showed different degrees of matrix deformation [Fig. 8(a)]. Within region I, located several hundred micrometers from the crack tip, the PBT matrix and the dispersed CSR fillers were not deformed by stress applied near the crack tip. In contrast, the TEM morphology within region II (several tens of micrometers from the crack tip) clearly showed both internal and interfacial cavities around the fillers; this resulted in deformation of the PBT matrix. In general, the cavitation process did not significantly contribute to the dissipation of the energy, which released the applied stress around the tip. However, it tended to produce sufficient driving force to deform the matrix; the cavities potentially transferred the stress field around the tip from plain strain to plain stress.[33,34] As shown in Figure 8(c), an intense white deformation zone was observed around the fractured surface, for example, in region III: the PBT matrix was significantly deformed along the direction considered to be the principal stretch axis. In particular, the loaded fillers were extensively elongated up to 10 of the original shape. As a result, the impact strength of the 0.4 wt % *g*GMA filler-loaded sample was greater by a factor of 12 compared to that of the homopolymer.

Because the rubber-toughened PBT blends showed lower ϕ_c values and crystal perfection of PBT with a decrease in τ, we suggest that below τ_c, the drastic increase in the Izod impact strength of the PBT blends was mainly related to the formation of less perfect lamellae around the particles. This was desirable because such lamellae readily deform under local stress and permit significant energy dissipation through substantial matrix deformation before fracture.

CONCLUSIONS

Semicrystalline PBT was melt-compounded with size-controlled rubber fillers, that is, CSR type PBA–PMMA (CSR) fillers. To minimize agglomeration of the CSR fillers in the low-viscosity PBT matrix during blending due to the low compatibility of the PMMA shell with the matrix, GMA, which reacted with the PBT chain ends, was grafted onto the outer shell of the fillers with a seeded emulsion polymerization. The TEM morphologies of the 20 wt % filler-loaded PBT blends showed that the dispersed rubber phases contained various aggregates with sizes ranging from about 0.3 to 2–3 μm, depending on the *g*GMA content in the filler. Thus, the values of τ of

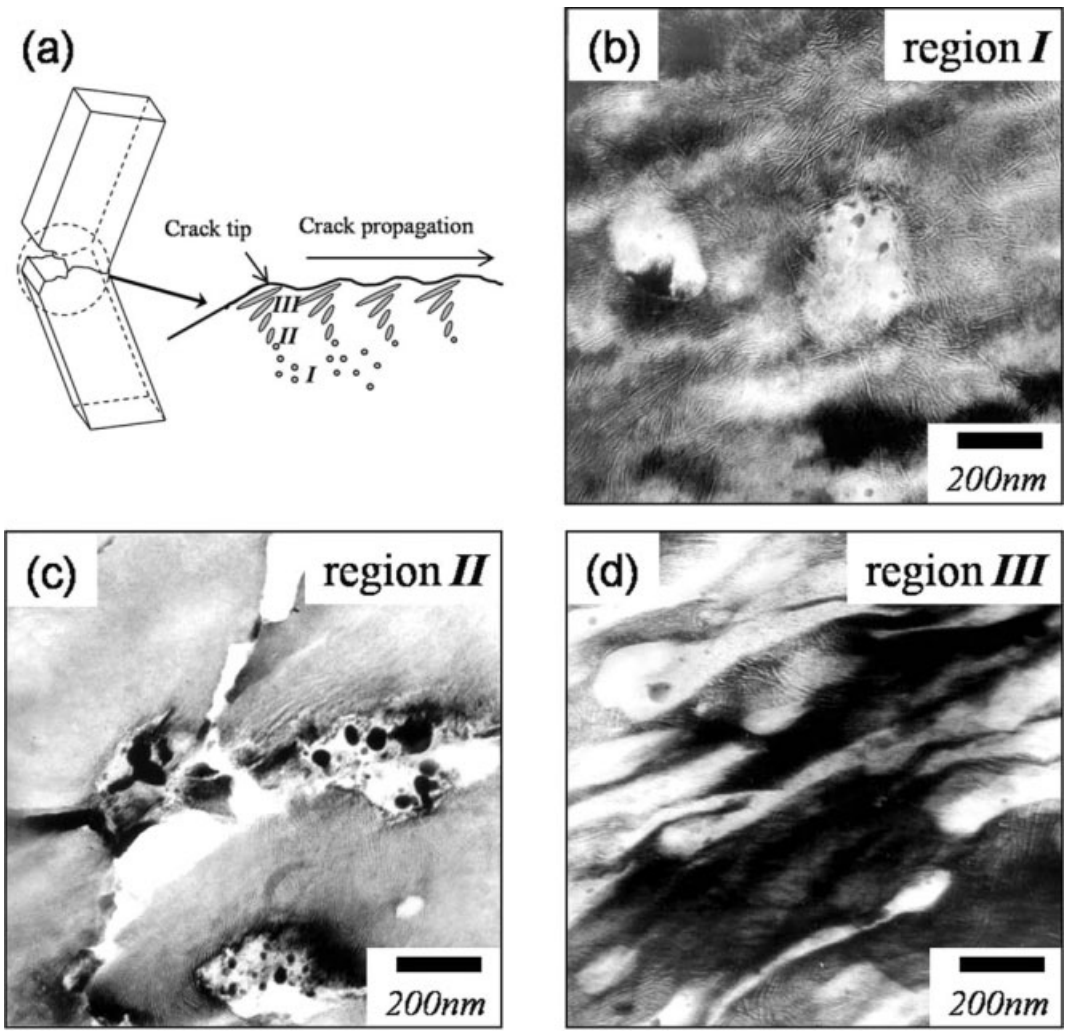

Figure 8 TEM micrographs of the various regions in the 0.4 wt % *g*GMA filler-loaded PBT blend sample used to measure the Izod impact strength.

the PBT blends could be controlled with the chemical reaction between *g*GMA and the matrix PBT for a fixed filler loading. The crystalline morphologies of the PBT blends were found to vary significantly with changes in the value of τ. At $\tau > 1$ μm, the PBT crystallites grew into 3-D spherulites, whereas for $\tau < 1$ μm, local confinement around the nearest fillers prevented the PBT chains from growing into spherulites. The Izod impact strengths of the samples at room temperature were found to be significantly higher for τ values below 0.4 μm. Nonisothermal DSC studies of the samples showed that ϕ_c of the matrix tended to decrease with increasing local confinement induced by the fillers and by the tethering of the PBT chains. Our results show that the significant increase in the toughness of the rubber-modified semicrystalline polymer blends below τ_c was connected to a structural transition of the matrix crystals, that is, to the presence of less ordered crystalline lamellae under significant geometrical confinement.

References

1. Wang, X. H.; Zhang, H. X.; Wang, Z. G.; Jiang, B. Z. Polymer 1997, 38, 1569.
2. Ishak, Z. A. M.; Ishiaku, U. S.; Karter-Kocsis, J. J Appl Polym Sci 1999, 74, 2470.
3. Mantovani, G. L.; Canto, L. B.; Hage, E.; Pessan, L. A. Macromol Symp 2001, 176, 167.
4. Arostegui, A.; Gaztelumendi, M.; Nazabal, J. Polymer 2001, 42, 9565.
5. Arostegui, A.; Nazabal, J. J Appl Polym Sci 2004, 91, 260.
6. Yu, Z. Z.; Yang, M. S.; Dai, S. C.; Mai, Y. W. J Appl Polym Sci 2004, 93, 1462.
7. Larocca, N. M.; Hage, E.; Pessan, L. A. Polymer 2004, 45, 5265.
8. Sun, S. L.; Xu, X. Y.; Yang, H. D.; Zhang, H. X. Polymer 2005, 46, 7632.
9. Oshima, J.; Fujii, T.; Tachibana, S. Kobunshi Ronbunshu 1995, 52, 46.
10. Hale, W.; Keskkula, H.; Paul, D. R. Polymer 1999, 40, 3353.
11. Hale, W.; Keskkula, H.; Paul, D. R. Polymer 1999, 40, 365.
12. Wu, J. S.; Wang, K.; Yu, D. M. J Mater Sci 2003, 38, 183.
13. Brady, A. J.; Keskkula, H.; Paul, D. R. Polymer 1994, 35, 3665.
14. Okamoto, M.; Shinoda, Y.; Kojima, T.; Inoue, T. Polymer 1993, 34, 4868.
15. Wu, S. H. J Appl Polym Sci 1988, 35, 549.
16. Arostegui, A.; Nazabal, J. Polymer 2003, 44, 5227.

17. Bartczak, Z.; Argon, A. S.; Cohen, R. E.; Weinberg, M. Polymer 1999, 40, 2331.
18. Bartczak, Z.; Argon, A. S.; Cohen, R. E.; Weinberg, M. Polymer 1999, 40, 2347.
19. Kanai, H.; Sullivan, V.; Auerbach, A. J Appl Polym Sci 1994, 53, 527.
20. Bartczak, Z.; Argon, A. S.; Cohen, R. E.; Kowalewski, T. Polymer 1999, 40, 2367.
21. Yang, H.; Bhimaraj, P.; Yang, L.; Siegel, R. W.; Schadler, L. S. J Polym Sci Part B: Polym Phys 2007, 45, 747.
22. Cho, K.; Yang, J. H.; Yoon, S.; Hwang, M.; Nair, S. V. J Appl Polym Sci 2005, 95, 748.
23. Friedrich, K.; Ueda, E.; Kamo, H.; Evstatiev, M.; Krasteva, B.; Fakirov, S. J Mater Sci 2002, 37, 4299.
24. Chen, W. P.; Zhu, M. F.; Song, S.; Sun, B.; Chen, Y. M.; Adler, H. J. P. Macromol Mater Eng 2005, 290, 669.
25. Hale, W. R.; Pessan, L. A.; Keskkula, H.; Paul, D. R. Polymer 1999, 40, 4237.
26. Kim, H. G.; Robertson, R. E. J Polym Sci Part B: Polym Phys 1998, 36, 1757.
27. Schonherr, H.; Frank, C. W. Macromolecules 2003, 36, 1188.
28. Schonherr, H.; Frank, C. W. Macromolecules 2003, 36, 1199.
29. Sakai, Y.; Imai, M.; Kaji, K.; Tsuji, M. Macromolecules 1996, 29, 8830.
30. Mellbring, O.; Oiseth, S. K.; Krozer, A.; Lausmaa, J.; Hjertberg, T. Macromolecules 2001, 34, 7496.
31. Stern, T.; Wachtel, E.; Marom, G. J Polym Sci Part B: Polym Phys 1997, 35, 2429.
32. Billon, N.; Magnet, C.; Haudin, J. M.; Lefebvre, D. Colloid Polym Sci 1994, 272, 633.
33. Muratoglu, O. K.; Argon, A. S.; Cohen, R. E. Polymer 1995, 36, 2143.
34. Muratoglu, O. K.; Argon, A. S.; Cohen, R. E.; Weinberg, M. Polymer 1995, 36, 4787.
35. Nichols, M. E.; Robertson, R. E. J Polym Sci Part B: Polym Phys 1992, 30, 755.
36. Nichols, M. E.; Robertson, R. E. J Polym Sci Part B: Polym Phys 1992, 30, 305.
37. Kulshreshtha, B.; Ghosh, A. K.; Misra, A. J Macromol Sci Phys 2003, 42, 307.
38. Yeh, J. T.; Runt, J. J Polym Sci Part B: Polym Phys 1989, 27, 1543.
39. Aerdts, A. M.; Groeninckx, G.; Zirkzee, H. F.; vanAert, H. A. M.; Geurts, J. M. Polymer 1997, 38, 4247.